Ocean Engineering 38 (2011) 2227–2243

Contents lists available at SciVerse ScienceDirect

Ocean Engineering

journal homepage: www.elsevier.com/locate/oceaneng

Second-order resonant heave, roll and pitch motions of a deep-draft semi-submersible: Theoretical and experimental results

V.L.F. Matos [a], A.N. Simos [b,*], S.H. Sphaier [c]

[a] PETROBRAS, E&P—Exploration and Production Department, Macaé, RJ, Brazil
[b] Tanque de Provas Numérico (TPN), Escola Politécnica—University of São Paulo, São Paulo, SP, Brazil
[c] Department of Ocean Engineering, COPPE/UFRJ, Rio de Janeiro, RJ, Brazil

ARTICLE INFO

Article history:
Received 3 January 2011
Accepted 8 October 2011
Editor-in-Chief: A.I. Incecik
Available online 10 November 2011

Keywords:
Semi-submersibles
2nd Order wave forces
Resonant motions
Numerical modeling
Experimental results
Validation

ABSTRACT

Large volume semi-submersible units may present significant wave induced resonant motions in heave, roll and pitch. Evaluating the slow motions of such systems is important from the initial stages of their designs and therefore requires a model that is both accurate and expedite enough. In the present article, different options for modeling the second-order hydrodynamic forces and induced motions are discussed using as a case-study the PETROBRAS 52 unit—P-52. Computations of the low frequency forces are performed in the frequency domain by means of a commercial Boundary Element Method (BEM) code. Different hydrodynamic approximations are tested and evaluated by directly comparing the predicted responses with those measured in small-scale tests performed in a wave-basin. From the results obtained in theses comparisons, a methodology based on a white-noise approach of the force spectrum is proposed. The validity of such approximation is attributable to the typically low damping levels in heave, roll and pitch motions. Furthermore, results also indicate that the second order forces may be calculated disregarding the free-surface forcing components, an option that helps to reduce the computational burden even more, rendering the procedure suitable for preliminary design calculations.

1. Introduction

Nowadays, the petroleum offshore industry is facing more and more challenging fields. Recently, PETROBRAS has discovered pre-salt reservoirs located about 300 km from the Brazilian coast in water depths around 2200 m. It will be necessary, in some cases, to drill wells 6000 m beneath the soil surface (10,000 m length) deviating them into salt layers with thicknesses around 2000 m. These wells will be very complex and an average time of approximately ninety days to drill them is expected. With the rig units market warmed up, the costs have increased considerably. In this scenario, production platforms fitted with rig capability have become very attractive.

An important requirement for a unit with drilling capabilities is the low level of motions in the vertical plane (motions induced by heave, roll and pitch). TLPs certainly fulfill this requirement, although the anchor system with tendons in 2200 m of water depth is a tremendous challenge. SPARs have the disadvantage of an offshore topside installation and integration that, in Brazilian waters, may cause serious construction delay problems. On the other hand, semi-submersible platforms seem to avoid the difficulties mentioned above while keeping the desired drilling capabilities in a production platform.

One of the manners to improve the hydrodynamic behavior of a semi-submersible is to increase the draft. Another important property that certainly will be necessary is a great displacement to withstand the weight of a modern rig with high hook up loads and a process plant. In fact, even before the pre-salt scenario, there was already a clear trend toward increasing draft and displacement of PETROBRAS' production-only semi-submersible units. This trend can be easily appraised by the data presented in Figs. 1 and 2, concerning the more recent designs. As will be discussed later, these two features together (deep draft and large displacement) tend to increase the second order heave, roll and pitch motions, which sometimes may present amplitudes comparable to the first order ones.

Bearing this scenario in mind, this work aims at performing a theoretical and numerical study to model and evaluate second order effects in the vertical plane motions with focus on semi-submersible platforms. In this study, hydrodynamic forces are computed in the frequency domain through the software WAMIT®, which calculates the hydrodynamic coefficients by solving the potential flow boundary-value problem. These computations, however, may be very time-consuming, particularly for the second-order problem. Therefore, in order to reduce the computational demands and accelerate the

* Corresponding author. Tel.: +55 11 30915112; fax: +55 11 30915717.
E-mail addresses: vmatos@petrobras.com.br (V.L.F. Matos), alesimos@usp.br (A.N. Simos), sphaier@peno.coppe.ufrj.br (S.H. Sphaier).

0029-8018/$ - see front matter © 2011 Elsevier Ltd. All rights reserved.
doi:10.1016/j.oceaneng.2011.10.005

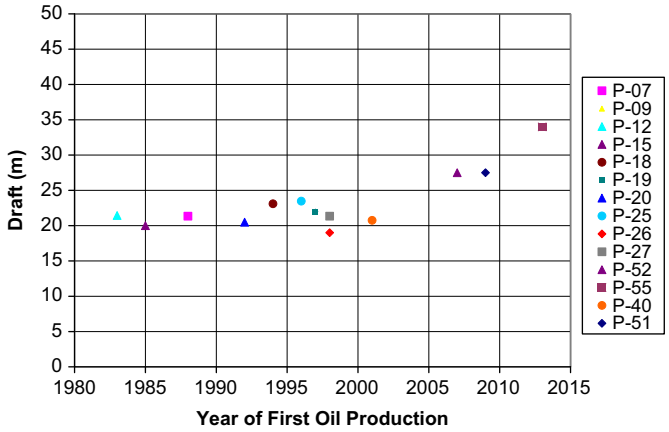

Fig. 1. Draft versus 1st Oil Production for PETROBRAS Semi-submersible units.

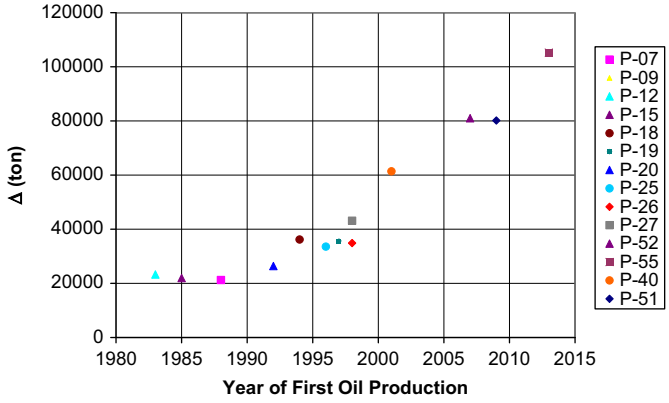

Fig. 2. Displacement with 1st Oil Production for PETROBRAS Semi-submersible units.

analysis, several approximations concerning the hydrodynamic model are tested and compared. Some of these consider the wave force computation itself, while others concern the dynamic model of the floating unit. Their validity is tested by confronting the predicted motions with those obtained in small-scale tests. Another issue that is addressed concerns the system damping; since one is dealing with resonant responses, the question of how to consistently consider the viscous damping deserves special attention. As a result of this research, it will be demonstrated that it is possible to establish a procedure that provides adequate predictions of the slow motions with relatively small computational effort.

2. Theoretical model

Low frequency second order loads are known to have significant influence on motions and mooring requirements of large floating structures. This is particularly true concerning the drift forces that act on the vessels and may cause resonant motions in the horizontal plane, the so-called slow-drift problem. Regarding vertical motions, the practical effects of mean or slow-motions are usually not of main concern compared to those induced by the large first-order loads, although Pinkster (1980) already expressed that large-volume, deep floating vessels might experience significant resonant motions. Evidences of slow roll motions of semi-submersibles were presented, for example, by Dallinga et al. (1988).

The mathematical model that represents the second-order loads in the six dofs of the body is very well detailed in the literature – see, for example, Pinkster (1980) and Ogilvie (1983) – and therefore only some essential aspects of the theory will be described here, as they will be required for a better comprehension of the hydrodynamic approximations that will be investigated ahead.

2.1. Boundary value problem

The velocity potential $\phi(x,y,z,t)$ is a solution of Laplace's Equation ($\nabla^2\phi=0$) and satisfies prescribed boundary conditions on the sea-floor, on the body surface, on the free-surface and the radiation condition. On the free-surface, kinematic and dynamic conditions need to be satisfied. By means of the standard expansion of the potential and free-surface elevation, the following pair of free-surface boundary conditions is obtained for the first and second-order problems (Pinkster, 1980):

$$g\frac{\partial\phi^{(1)}}{\partial z}+\frac{\partial^2\phi^{(1)}}{\partial t^2}=0 \tag{1}$$

$$\frac{\partial^2\phi^{(2)}}{\partial t^2}+g\frac{\partial\phi^{(2)}}{\partial z}=-\frac{\partial}{\partial t}|\nabla\phi^{(1)}|^2+\frac{1}{g}\frac{\partial\phi^{(1)}}{\partial t}\frac{\partial}{\partial z}\left(\frac{\partial^2\phi^{(1)}}{\partial t^2}+g\frac{\partial\phi^{(1)}}{\partial z}\right) \tag{2}$$

where $\phi^{(1)}$ and $\phi^{(2)}$ are, respectively, the first and second-order potentials, g is the gravitational acceleration, and both equations are to be solved on the mean (fixed) free-surface ($z=0$). It may be readily seen in Eq. (2) that the second-order problem is forced by the first order solution. Also, it is important to mention that, in terms of the numerical solution obtained via BEM, the non-homogenous free-surface second order boundary condition requires a numerical discretization of the free surface, which greatly increases the computational effort.

2.2. Second order loads

When the hydrodynamic forces are obtained by direct integration of the pressure on the body surface, the derivation of the second order loads requires the pressure and body normal vectors to be expanded through the same perturbation technique. Following Pinkster (1980), the integral of the product of pressure forces on the body surface generates five second order components for the hydrodynamic exciting loads. These components are due to the following:

I. first order relative wave elevation,
II. quadratic components of the first order velocities,
III. products of the gradient of first order pressure and first order motions,
IV. rotation of the first order fluid force relative to the body axes (which may also be written in terms of the first order body inertial forces),
V. second order potential.

Only the fifth component has the contribution of the second order potential that needs to satisfy Eq. (2) and requires significant numerical effort, as described before.

Let (ω_i,ω_i) be any pair of wave frequencies considered in the discrete wave spectrum. Lee et al. (1991) present how to calculate the component V for each mode α through the so-called direct method:

$$\vec{F}^{(2-)}_{5,\alpha}=-i\rho(\omega_i-\omega_j)\iint_{S_0}(\phi_I^{(2-)}+\phi_S^{(2-)})n_\alpha dS \tag{3}$$

where $\phi_I^{(2-)}$ and $\phi_S^{(2-)}$ are the incident and scattered waves contributions of the second-order potential, respectively, n_α stands for the corresponding components of the mean normal vector $\vec{n}$ for translation modes $\alpha=1,2,3$ or to the components $(\vec{x}\times\vec{n})_{\alpha-3}$ for rotation modes $\alpha=4,5,6$ and S_0 is the mean body surface.

Alternatively, Faltinsen and Loken (1978), Lighthill (1979) and Molin (1979) introduced the indirect method, in which the same component may be obtained without the need to calculate the second-order scattered wave potential, as follows:

$$\vec{F}_{5,\alpha}^{(2-)} = -i\rho(\omega_i-\omega_j)\left[\iint_{S_0}(\phi_I^{(2-)}n_\alpha+\phi_\alpha^{(-)}Q_B^{(-)})dS+\frac{1}{g}\iint_{S_{FS}}(Q_{IB}^{(-)}+Q_{BB}^{(-)})\phi_\alpha^{(-)}dS\right] \tag{4}$$

where $Q_B^{(-)}$ is the low-frequency forcing function on the body surface, $(Q_{IB}^{(-)}+Q_{BB}^{(-)})$ is a component of the free-surface forcing function, both computed from the first order solution and $\phi_\alpha^{(-)}$ is the first order radiation potential for the motion α computed in the difference-frequency. Details concerning the derivation and computation of Eq. (4) by WAMIT® can be obtained in Lee (1995).

Eqs. (3) and (4) represent the same physical forces calculated by different approaches. WAMIT® allows the computations to be performed by both methods, and the agreement between their results is also a check of the numerical convergence with respect to the mesh size.

2.2.1. Second order loads in irregular seas

The difference-frequency second order forces induced by irregular waves may be computed by means of the so-called quadratic transfer function (QTF):

$$\vec{F}_{\alpha}^{(2)}(t) = \sum_{j=1}^{N}\sum_{k=j}^{N}A_jA_k^*T_\alpha(\omega_j,\omega_k)e^{-i(\omega_j-\omega_k)t}+(*) \tag{5}$$

where the complex function $T_\alpha(\omega_j,\omega_k)$ represents the QTF for the motion in dof α (see, for instance, Pinkster (1974)) and * stands for the complex conjugate of the double summation in (5). Defining the difference frequency $\mu=\omega_j-\omega_k$, the QTF values can be rewritten as

$$T_\alpha(\omega_i;\omega_j)\equiv T_\alpha(\omega;\omega+\mu) \tag{6}$$

Obviously, the diagonal of the QTF matrix ($\mu=0$) corresponds to the mean wave-drift forces for frequency ω ($D_\alpha(\omega)$):

$$T_\alpha(\omega,\omega)=D_\alpha(\omega) \tag{7}$$

2.3. Second order response statistics

We are ultimately interested in the resonant motions of the floating unit that might be induced by the low-frequency second order loads $T_\alpha^{(-)}(\omega_i;\omega_j)$ in different sea conditions. In order to evaluate the magnitude of such motions, a spectral analysis will be performed considering both the first and second order force spectra.

The second order force spectrum is computed by crossing the QTF and wave spectrum $S(\omega)$, as showed next—see Pinkster (1974):

$$S_{F,\alpha}^{(-)}(\mu)=8\int_0^\infty S(\omega)S(\omega+\mu)\left|T_\alpha^{(-)}(\omega;\omega+\mu)\right|^2d\omega \tag{8}$$

Once the force spectrum is computed for a particular sea condition, the second order low-frequency response spectrum for the degree of freedom α ($S_\alpha^{(-)}(\omega)$) is determined by the product of the squared unitary force transfer function ($H_{\alpha k}(\omega)$) and the spectrum defined in (8):

$$S_\alpha^{(-)}(\omega)\cong\left|H_{\alpha k}(\omega)\right|^2S_{F,\alpha}^{(-)}(\omega) \tag{9}$$

where

$$H_{\alpha k}(\omega)=\frac{1}{-\omega^2(M_{\alpha k}+A_{\alpha k}(\omega))+i\omega(B_{\alpha k}(\omega)+B'_{\alpha k})+(C_{\alpha k}+C'_{\alpha k})} \tag{10}$$

This transfer function encloses all the dynamic characteristics of the floating body, A, B and C being, respectively, the added mass, potential damping and hydrostatic restoration matrixes, with α and k varying from 1 to 6. $B'_{\alpha k}$ is the viscous damping and C'_{kj} is the external stiffness induced, in this case, by mooring lines and risers.

With the second order response spectrum $S_\alpha^{(-)}(\omega)$, the spectral density moments can be calculated in the following way:

$$m_k=\int_0^\infty\omega^kS_\alpha^{(-)}(\omega)d\omega \tag{11}$$

where k indicates order of the moment, by means of which the usual statistical parameters of the response may be estimated, as for example,

- Variance of the response in dof α:

$$m_0=\int_0^\infty S_\alpha^{(-)}(\omega)d\omega \tag{12}$$

- Significant amplitude and height:

$$A_S=2\sqrt{m_0} \tag{13}$$

$$H_S=4\sqrt{m_0} \tag{14}$$

2.4. Hydrodynamic approximations

So far, emphasis was given on discussing the main formulation of the theoretical potential flow model that describes how we can estimate the resonant second order response in a particular sea condition. In order to apply this model for the semi-submersible unit, the QTF must be computed numerically. For instance, the program WAMIT® computes the QTF values based on the boundary-integral-equation "panel" method, using free-surface Green functions—see Lee and Newman (2004). However, as mentioned before, the QTF calculation requires considerable computational effort and may encompass a large number of frequency combinations—see Eq. (8). Therefore, in order to avoid unnecessary computational effort, mainly in the initial stages of the floating system design, a number of possible approximations proposed in literature for dealing with low-frequency problems was tested and will be described next. Some of these (Sections 2.4.1–2.4.3) consider simplifications in the QTF computation, while others (Sections 2.4.4 and 2.4.5) make use of particular characteristics of the system dynamics to propose approximations in the force spectrum calculation. It is important to notice that, as they are based on different physical aspects of the problem, some of these simplifications may eventually be combined to further reduce the computational burden.

2.4.1. QTF without free-surface forcing terms

The first approximation is discussed, for instance, in WAMIT® user manual (WAMIT, 2006) and consists on solving the second order problem without the evaluation of the free surface integral. This means that the second order potential, instead of Eq. (2), will satisfy the homogeneous second order free-surface boundary condition:

$$\frac{\partial^2\phi^{(2)}}{\partial t^2}+g\frac{\partial\phi^{(2)}}{\partial z}=0 \tag{15}$$

The advantage of this approximation is that, if it indeed proves valid to the particular boundary value problem considered, free-surface discretization would no longer be required and computation of the second-order potential would therefore be much faster. The WAMIT® manual alerts that this approximation depends on the particular problem and that this option should be used with discretion.

2.4.2. QTF without the contribution of the 2nd order potential

The second one, that WAMIT® permits as well, is to calculate the QTFs without the inclusion of the Component V in the total force, that is, disregarding the contribution of the second

order potential. Obviously, this approach is only reasonable if the second order forces that induce the resonant motions are dominated by the quadratic first order components. As this approximation only needs the solution of the first order problems, it is even faster than the simplification discussed in Section 2.4.1.

2.4.3. Newman's approximation

Newman's approximation (1974) is frequently adopted for modeling the slow-drift problem of moored floating vessels. By this proposal, the QTF values are obtained through the following formulation:

$$T_{\alpha}^{(-)}(\omega,\omega+\mu)=D_{\alpha}(\omega+\mu/2) \tag{16}$$

Aranha and Fernandes (1994) later demonstrate that, when $\mu\cong\mu_n=\omega_n$ and $\mu_n\ll 1$, the approximation above has an error with order of magnitude of $O(\mu_n^2)$. This is often the case of moored floating systems, for which the natural periods of surge, sway and yaw are in general above 100 s. As the mean drift forces can be obtained by the solution of first order problem, approximation (16) permits to estimate the slow drift forces in the horizontal plane in a simple and expedite way. This methodology also avoids the computation of a great number of frequency combinations, therefore reducing the computational effort. Nevertheless, when dealing with the semi-submersible motions in the vertical plane, one must have in mind that the natural periods of heave, roll and pitch are in the range of 20 to 80 s, considerably lower than the typical values observed for the horizontal motions. Thus, as the error increases with $O(\mu_n^2)$, the application of Newman's approximation for estimating the resonant motions in the vertical plane may not be advisable.

2.4.4. White-noise approximation

The statement above inspired the use of another approach in the present work: the white noise approximation, a classical methodology proposed by Crandall and Mark (1963) for the analysis of mechanical systems with narrow band response. The semi-submersible motions in the vertical plane are characterized by having very low damping values. Due to this, their response spectrums are usually narrow-banded, with a pronounced energy peak in the natural frequency. The dynamic characteristics of the system therefore indicate that the second-order response spectrum (9) may be computed considering a white-noise approximation of the force spectrum (8), hence

$$S_{\alpha}^{(-)}(\omega)\cong|H_{\alpha k}(\omega)|^2 S_{F,\alpha}^{(-)}(\omega_{n,\alpha}) \tag{17}$$

where $\omega_{n,\alpha}$ is the natural frequency of the motion α. By doing this, it is admitted that the force spectrum may be regarded as approximately constant (in the narrow band of frequencies with significant response) and equal to its value calculated in the natural frequency of motion. The advantage of this approach is then obvious: the second-order force spectrum must be computed only for one difference-frequency $\mu=\mu_n=\omega_{n,\alpha}$:

$$S_{F,\alpha}^{(-)}(\omega_{n,\alpha})=8\int_0^{\infty}S(\omega)S(\omega+\omega_{n,\alpha})|T_{\alpha}^{(-)}(\omega;\omega+\omega_{n,\alpha})|^2 d\omega \tag{18}$$

The white-noise approximation reduces the computational effort taking advantage of the characteristics of the system dynamics. It does not impose any condition of the computation of the QTF. Thus, for instance, if the hydrodynamic problem allows the second-order potential contribution to be neglected, it may be combined to the simplification discussed in Section 2.4.2 in order to speed-up the analysis even further.

It is also important to notice that the white-noise approximation has been used before in this context. Dallinga et al. (1988), for example, made use of this approach to evaluate the slow roll motions of semi-submersibles.

2.4.5. Decoupled unitary force transfer functions

One final simplification that is considered concerns the computation of the so-called unitary force transfer function $H_{\alpha}(\omega)$. If the coupling effects in the vertical motions are small, then the response spectrum can be given by

$$S_{\alpha}^{(-)}(\omega)\cong|H_{\alpha}(\omega)|^2 S_{F,\alpha}^{(-)}(\omega) \tag{19}$$

with

$$H_{\alpha}(\omega)=\frac{1}{-\omega^2(M_{\alpha\alpha}+A_{\alpha\alpha}(\omega))+i\omega(B_{\alpha\alpha}(\omega)+B'_{\alpha\alpha})+(C_{\alpha\alpha}+C'_{\alpha\alpha})} \tag{20}$$

Eqs. (19) and (20) include only the coefficients in the main diagonal of the mass, damping and stiffness matrixes. This simplification will be more precise the weaker the coupling effects between the motions are.

In this section, different approximations that may be taken into consideration for dealing with the second order resonant motions of a semi-submersible were presented. Undoubtedly, the use of any of these approximations will result in a significant gain in terms of time and computational efforts. It was also emphasized that some of these simplifications may be combined; for example, the white-noise approach can be employed with QTF values computed without the evaluation of the free-surface forcing terms and with a decoupled unitary force transfer function for the motion α. However, as stated before, the validity of each of one of these approaches must be previously evaluated by confrontation with experimental results and this is the aim of the following sections.

3. Case-study: the P-52 unit

An evaluation of the second-order resonant roll, pitch and heave motions was performed for the PETROBRAS 52 (P-52—see Fig. 3) unit, the largest semi-submersible production platform operating in PETROBRAS fleet. P-52 was installed in Roncador

Fig. 3. Picture of P-52 just after deck matting operation.

Field (Campos Basin) in October 2007. It is moored in a water depth of approx. 1.800 m through a mooring system composed of 16 lines in taut-leg configuration. The platform heads North.

All experimental and numerical data and results presented in this section are in real scale and the spectral density functions were evaluated base on the cross spectral density estimative of the time series through the Welch method (that uses Fast Fourier Transform – FFT – applied to the data).[1]

The degrees of freedom (DOF) indicated in the graphics represent DOF=N/M, where N is the number of observations in the original time series and M is the maximum lag in the autocorrelation function that uses the basis for the FFT.

3.1. Model tests

The first time relevant second-order resonant motions in the vertical plane were observed in PETROBRAS FU designs was during P-52 model tests. These tests were conducted in 2002, in the Norwegian Marine Technology Research Institute (Marintek) ocean basin. P-52 model scale was 1:100. Its main properties (in real scale) are presented in Table 1.

The P-52 model tests program included many types of mooring and lines configurations (with horizontal mooring, truncated mooring lines only, truncated mooring lines with risers), two different wave conditions (with and without a 100 y.r. current and wind) and also different wave headings. However, as the main objective here is to evaluate the resonant vertical motions induced by waves, only one case will be considered next: the one with the model moored with a soft horizontal mooring and a head wave condition generated without wind and current.

Regarding the wave condition, the Campos Basin 100 y.r. wave considered here is represented by a JONSWAP spectrum with H_S=6.3 m, T_p=10 s and γ=2.4. Fig. 4 shows the wave elevation time series measured at the model position and Fig. 5 brings its respective spectrum density function, compared to the theoretical wave spectrum. In Fig. 6, the time series of the measured pitch motion is printed. P-52 model was submitted to the wave of Fig. 4 for a period equivalent to 3.5 h and the data acquisition rate corresponded to 4 Hz (real scale). The first half hour was discharged in order to avoid the influence of transient effects.

A spectral analysis of the pitch time series was performed and the results are printed in Fig. 7. Note that the spectrum peak on the natural period reduces significantly with the aliasing of the spectral density function, or, in other words, with the degrees of freedom (DOF) of the spectral analysis—see also Fig. 9. In addition, the spectral bandwidth of the resonant response tends to increase with the aliasing. Nonetheless, the results in Fig. 8 show that despite the variations in spectral peak and band, the zero-order moment m_0 remains almost constants with the DOF. Results in Fig. 8 were generated in the following manner:

- For each spectral density function calculated with different aliasing levels (DOF), the spectrum area (m_0 – Eq. (12) – variance) in the wave frequency range (from 5 to 20 s) was obtained. It is represented by the red curve—1st order.
- The same calculation was then performed for periods ranging from 20 to 57 s, and results are represented by the black curve—2nd order.
- The green curve was generated by calculating the values of m_0 for all frequencies considered in the spectral analysis.

[1] The spectral density functions are smoothed by a Hanning type window with 50% of overlap.

Table 1
Main properties of P-52 model.

Length (m)	120.0
Beam (m)	110.0
Draft (m)	27.5
Volume (m^3)	79000.0
Displacement (t)	80975.0

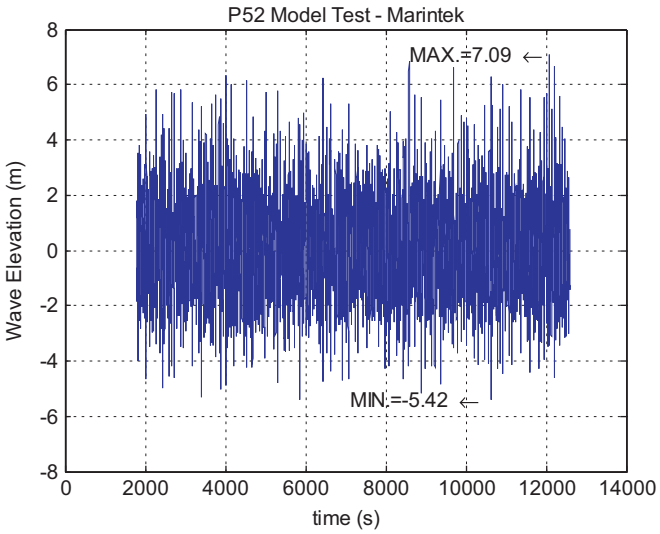

Fig. 4. Measured wave elevation time series in the model position.

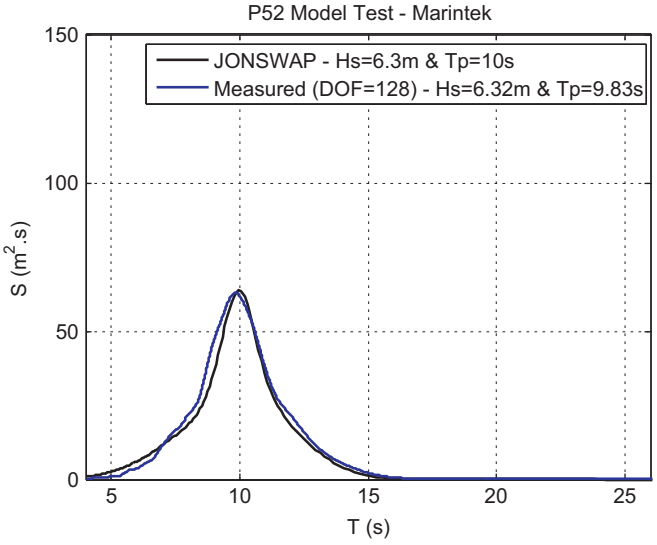

Fig. 5. Comparison of the theoretical wave elevation spectral density and the measured one.

- Finally, the magenta curve was obtained by evaluating the statistical variance in the time series:

$$\sigma^2 = \frac{\sum_{i=1}^{n} (x_i - \bar{x})^2}{n-1} \tag{21}$$

n being the number of data in the time series, x_i the measured values and $\bar{x}$ the mean value. As Eq. (21) is not computed by spectral analysis, this value was considered constant and was included in Fig. 8 as a reference.

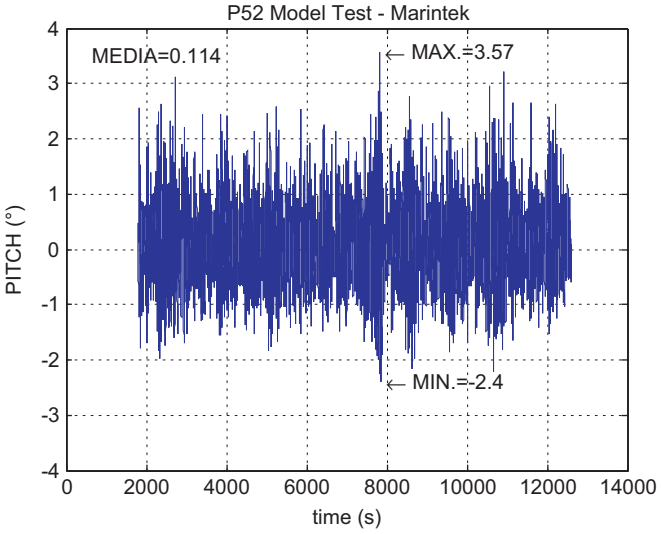

Fig. 6. Measured pitch time series.

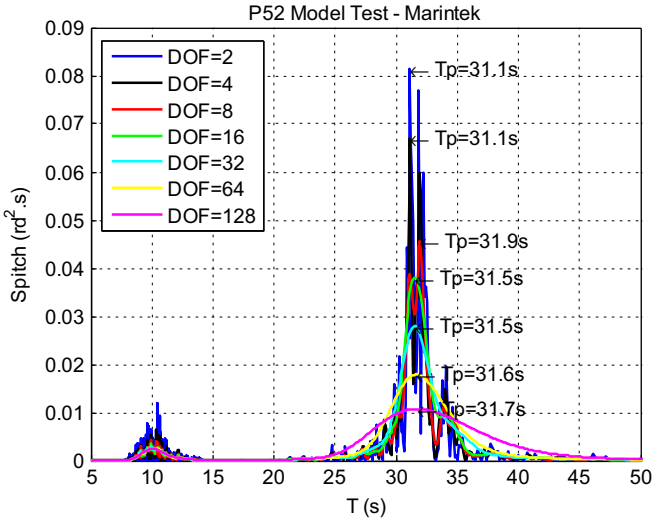

Fig. 7. Pitch spectral density function.

In Fig. 8 one can observe that the energy computed for the different frequency ranges vary just slightly with the DOF. The same is obviously not true regarding the spectrum peak value in the natural period of the motion (see Fig. 9). This means that, independent from the chosen aliasing, the comparison between experimental and numerical results should be performed based, for example, on the significant amplitude $2\sqrt{m_0}$ of the resonant motions. Also, as it should be expected, the summation of areas of the first and second order range spectral density is equivalent to the variance calculated with Eq. (21). This indicates that the total energy is well represented by the spectral density function, which is also not affected by the level of aliasing.

One should also notice from Fig. 7 that the resonant period identified from the spectral density function varies a little with the DOF. This can be explained by the fact that the aliasing changes the frequency discretization and the spectral peak as well. Nevertheless, this variation is very small and considering that the peak period coincides with the natural pitch period is a reasonable estimative.

Considerations above regarded pitch motions, however, similar conclusions can be drawn from the analysis of the heave signal measured in the tests (see Figs. 10–13).

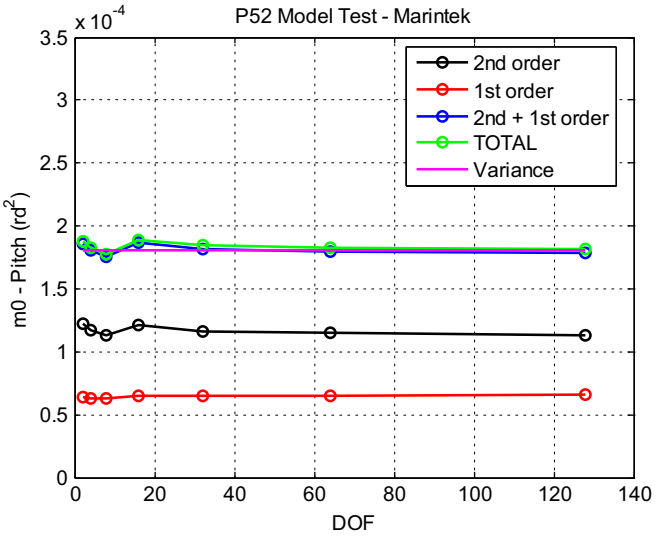

Fig. 8. m_0 Variation with spectral analysis degrees of freedom.

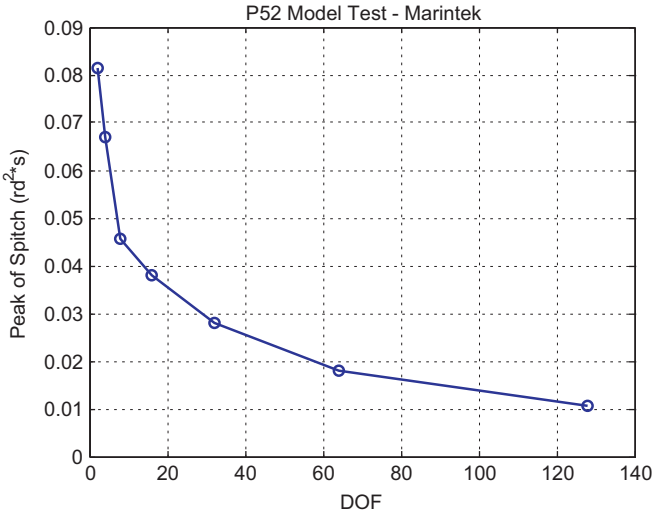

Fig. 9. Variation of the spectral density function peak for the pitch signal with DOF of the spectral analysis.

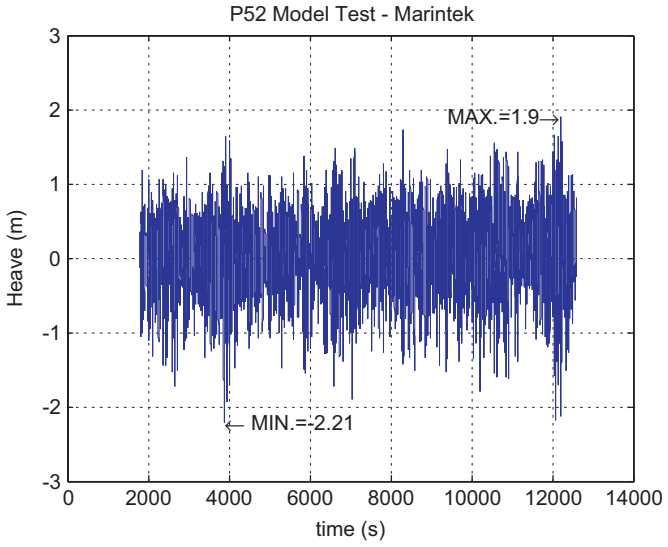

Fig. 10. Measured heave time series.

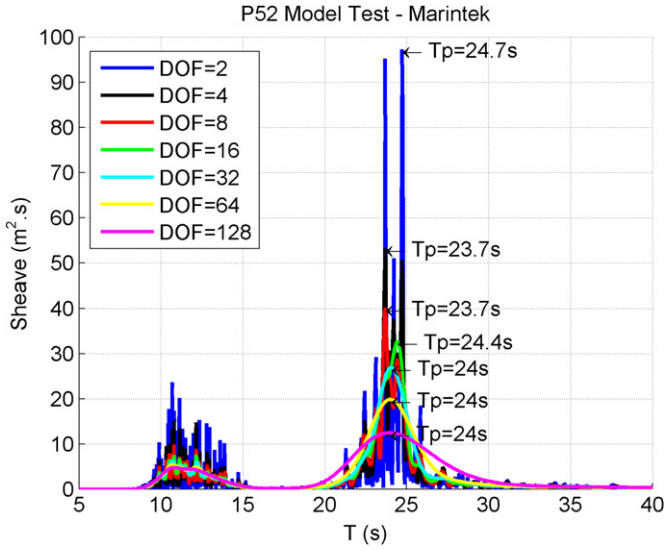

Fig. 11. Heave spectral density function.

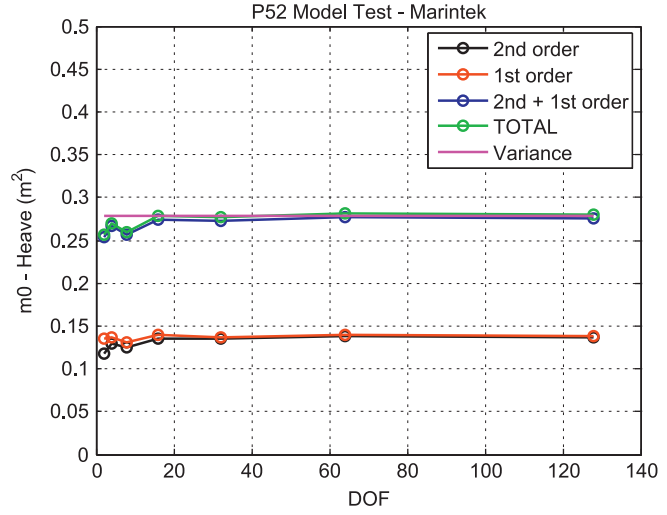

Fig. 12. m_0 Variation with spectral analysis degrees of freedom.

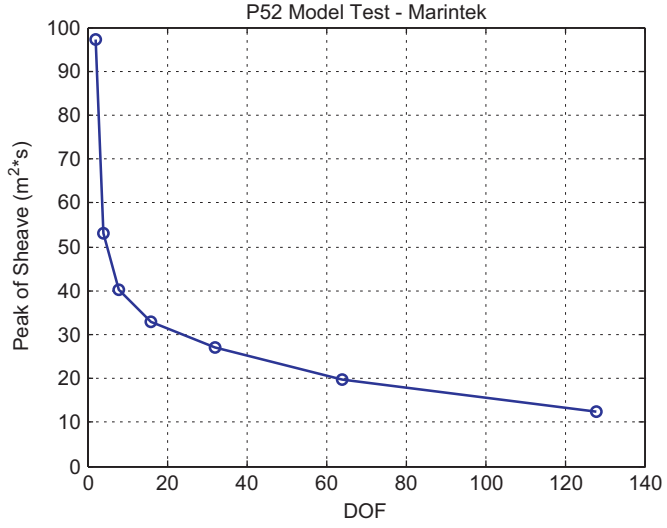

Fig. 13. Variation of the spectral density function peak for the heave signal with DOF of the spectral analysis.

3.2. Numerical model

This section describes the numerical models employed for estimating the 1st and 2nd order wave induced forces and motion spectra, considering the alternatives discussed in Section 2.4. All the hydrodynamic coefficients were computed by WAMIT®.

The second order spectral density function was calculated with different approaches.

3.2.1. Definition of frequencies

Observing Eq. (8), it is clear that one only needs to compute the quadratic transfer functions in the range of frequencies where there is considerable energy of the wave group spectrum $S(\omega)S(\omega+\mu)$. Hence, it is possible to define a frequency range of interest with respect to the frequency difference μ. As a criterion, it was adopted the range for which the value of $S(\omega)S(\omega+\mu) > 1/1000\text{MAX}(S(\omega)S(\omega+\mu))$, for each value of μ. Fig. 14 illustrates the range of periods selected by the criterion above for the wave condition considered in this analysis. Blue and red curves indicate the lowest (ω_i) and highest (ω_j) frequencies adopted, respectively, both with respect to the difference-frequency $\mu=\omega_j-\omega_i$

The frequency difference (μ) values were chosen to encompass both resonant periods, for the heave and pitch motions (Figs. 7 and 11). The following range was then selected: $18 < 2\pi/\mu < 57$ s. This range is also indicated in Fig. 14 by means of the black vertical lines.

3.2.2. Geometrical model and properties

The following procedure was adopted to estimate the model properties:

- The total mass was considered as the volume obtained by the numerical model multiplied by the water mass density.
- The vertical position of the center of gravity (CG) was calibrated in order to match the GMt value specified in Marintek (2002). Regarding its horizontal position, the CG was considered to be located amidships in the central plane.
- The pitch inertia (M55) and external stiffness (C′55) were chosen as the pair that provided the best agreement with the first-order motions measured in the experiments while keeping the numerical natural pitch period (Tn5) equal to the peak

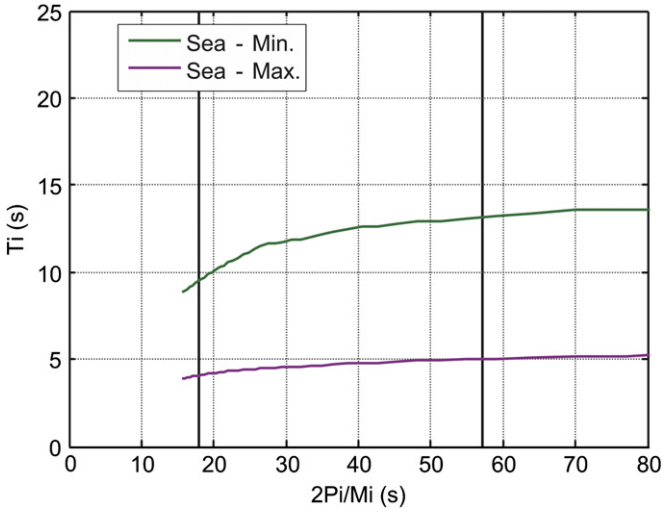

Fig. 14. Frequency range definition for the numerical analyses. (For interpretation of the references to color in this figure legend, the reader is referred to the web version of this article.)

Table 2
Main properties of P-52 numerical model.

Test	5130
M33 (t)	79695.9
M44 (t m^2)	107271411.5
M55 (t m^2)	103404299.4
M66 (t m^2)	103404299.4
Kxx (m)	35.7
Kyy (m)	36.0
KG (m)	25.0
GMt (m)	4.7
GMl (m)	6.5
C′11 (kN/m)	876.3
C′22 (kN/m)	867.9
C′44 (kN m/rd)	2762200.0
C′55 (kN m/rd)	1739700.0
C′66 (kN m/rd)	3156800.0
Tn3 (s)	23.7
Tn4 (s)	33.0
Tn5 (s)	31.5
Tn6 (s)	45.9

period estimated from the second-order spectral density function obtained from the tests data.

The main properties considered in P-52 numerical model are presented in Table 2. As a result of the procedure adopted for the calibration of the numerical model, the natural periods in heave and pitch corresponded to 23.7 s and 31.5 s, respectively.[2]

The P-52 geometric model was built using the software Multisurf® (Multisurf, 2008), with a mesh of 1928 panels (low order method—see WAMIT (2006)). Fig. 15(a) shows a picture of the geometric model representing the P-52 hull below the design water line, while Fig. 15(b) presents an illustration of the free-surface mesh (required for the computation of the 2nd order velocity potential), which was modeled with 12,256 panels in a circular configuration (the radius of this mesh is 200 m). Several tests were performed to evaluate the convergence of the numerical results based on these meshes. Fig. 16 provides an illustration of the convergence of numerical results as the number of panels on the body surface is increased. Results refer to the pitch and heave QTFs, both for difference-frequencies close to the respective natural frequencies and second-order potential contribution computed by the direct method according to Eq. (3).

3.2.3. QTF calculation

In Fig. 17, it is possible to visualize the P-52 QTF ($T_\alpha^{(-)}(\omega,\omega+\mu)$) values for heave (a) and pitch (d) computed by WAMIT® by solving the full second-order problem. The diagonal line in the central part of the figure represents the QTF values for $\mu=0$, which correspond to the mean drift forces. The area above the diagonal line contains the QTF values for the difference-frequencies (fi − fj). The QTFs are symmetrical with respect to the diagonal $\mu=0$.

The QTF values for constant μ values are represented by lines that are parallel to the main diagonal. As the value of μ increases, these lines are shifted away from the main diagonal ($\mu=0$).

The graphics (b) and (e) show the computed values for the wave group spectrum $S(\omega)S(\omega+\mu)$, whereas (c) and (f) present the values for the product $S(\omega)S(\omega+\mu)\left|T_\alpha^{(-)}(\omega;\omega+\mu)\right|^2$, where $S(\omega)$ is the wave spectrum as showed in Fig. 5. It should be noticed that, by integrating

[2] Regarding the heave natural period, it should be noted that small discrepancies in the natural period were verified when comparing the numerical and experimental response spectra, but those were small (around 0.5 s) and therefore considered acceptable.

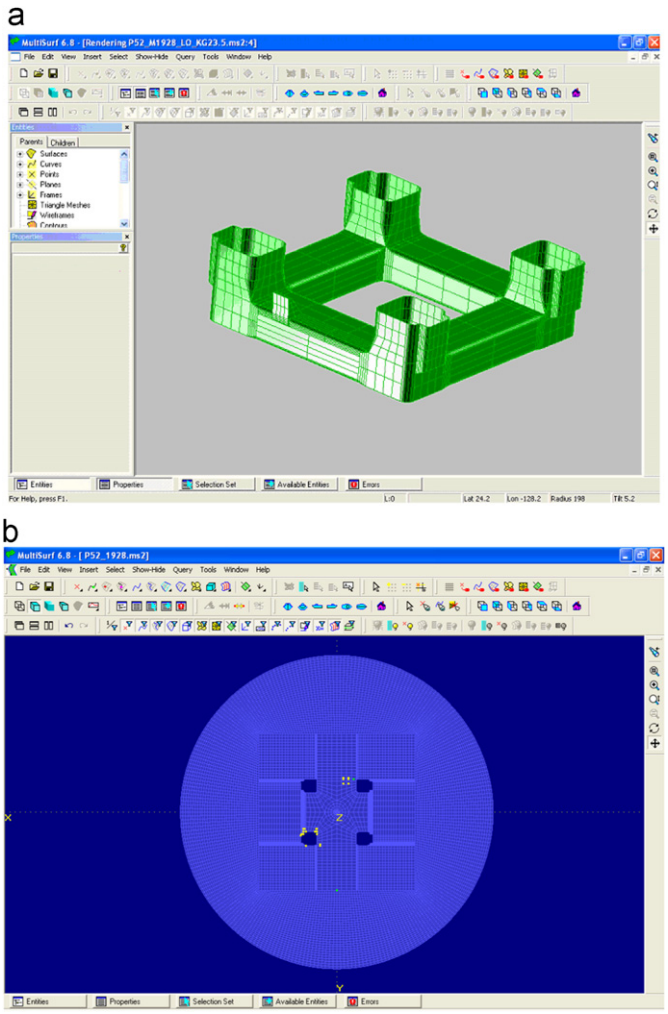

Fig. 15. (a) P-52 geometric mesh with 1928 panels; (b) Illustration of the free-surface mesh.

the product $S(\omega)S(\omega+\mu)\left|T_\alpha^{(-)}(\omega;\omega+\mu)\right|^2$ with respect to the frequency ω, the 2nd order force spectrum in the difference-frequency μ is obtained (Eq. (18)), which, if multiplied by the unitary force transfer function squared, generates the response spectral density function (Eq. (19)).

The area between the dotted lines represent the ranges of frequency difference for which significant 2nd order heave and pitch motions were observed in the model tests, thus the calculation of (8) is necessary only in these regions.

In Figs. 18 and 19, the QTF values are plotted in a different way for a better visualization of the influence of the approximations employed to calculate them (discussed in Section 2.4). The output QTF data from WAMIT® second-order module is printed in files with the following extensions:

- "filename.10d" – Quadratic second order loads – see Section 2.4.2.
- "filename.11d" – Total second-order loads by indirect method – see Eq. (4).
- "filename.12d" – Total second-order loads by direct method – see Eq. (3).

The letter "d" in the filenames means that these files contain the difference-frequency output. In the following graphics, the expression "without FS" indicates that QTF values were evaluated without the free-surface forcing terms, as explained in Section 2.4.1.

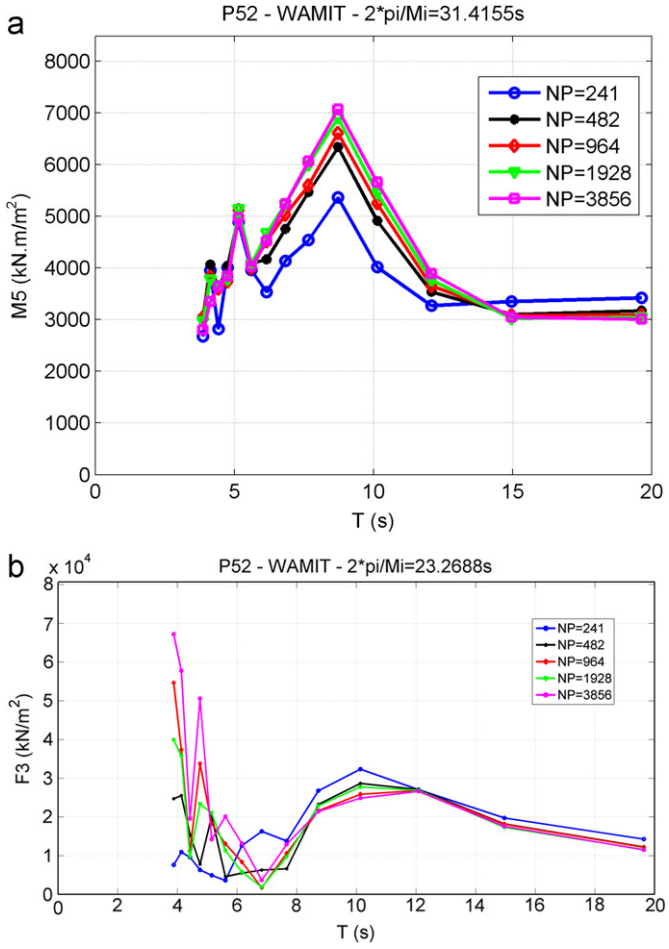

Fig. 16. Pitch (a) and heave (b) QTFs for body meshes of different sizes. NP indicates the number of panels on the body.

Concerning the 2nd order pitch moment (Fig. 18), it should be noticed that the frequency-difference μ corresponding to 31.4 s is the pitch natural period estimated for the P-52 model. The good agreement between the computations made with the direct and indirect methods indicates that a good numerical convergence was achieved. More importantly, it is easy to observe that the pitch QTF computed disregarding the second-order potential contribution (WAMIT-10d) differs considerably from the ones that take its influence into account (WAMIT-11d and 12d). On the other hand, the approximation without the free-surface forcing terms seems to agree quite well with the full computations in the frequency range around the natural frequency. As the low-frequency response is indeed narrow-banded due to the low damping values, the errors in the computed motions end up being small. As this latter approximation does not require the free-surface discretization, it saves computational and may be considered as an option when dealing with similar hulls. Similar conclusions can be drawn regarding the heave motions (Fig. 19).

3.3. Comparison of experimental and numerical results

As discussed before, the resonant motions are significantly affected by the level of damping inherent to the dynamical system. In order to evaluate this influence, the pitch response second-order spectral density functions were computed with different viscous damping ratios ζ_v. For that, the second-order pitch RAO ("filename.16d") considering the full QTF computations was used:

$$S_{\alpha}^{(-)}(\mu) = 8\int_0^{\infty} S(\omega)S(\omega+\mu)\left|\mathrm{RAO}_{\alpha}^{(2-)}(\omega;\omega+\mu)\right|^2 d\omega \tag{22}$$

where $S(\omega)$ is the wave spectrum measured at the P-52 model position (see Fig. 5).

One important aspect that should be remembered here is related to the changes in the resonant peak of the motion spectrum, which is reduced with the increase of the smoothness (see Figs. 7 and 9) or, in other words, with the increase of the DOF employed in the spectral analyses. For this reason, the experimental results in Fig. 20 were obtained, in this case, by finding the DOF that best fit the numerical computations. As it can be seen, by choosing an appropriate value of DOF, a good agreement can always be obtained, despite the viscous damping ratio that is considered. Therefore, the question that remains is then how to properly consider the viscous damping. The answer is related to the statement that m_0 does not vary significantly with the DOF (see Fig. 8). Results in Table 3, based on the m_0 computations, indicate that the viscous damping ratio that better reproduces the experimental results is $\zeta_v = 3.5\%$.[3]

All the computations concerning the pitch motions showed ahead in this paper have thus considered this value of $\zeta_v = 3.5\%$.

In Fig. 21, it is possible to observe the comparison of the pitch moment spectral density calculated according to Eq. (8) and those with QTF computed with the three different hydrodynamic approximations considered herein[4]:

(a) full second-order potential—curves of Fig. 18 with green or magenta color (output data file "0.11d" or "0.12d" from WAMIT®);
(b) second-order potential without the free-surface forcing terms—curves of Fig. 18 with black or yellow color (output data file "0.11d" or "0.12d" from WAMIT®);
(c) disregarding the second-order potential contribution—curves of Fig. 18 with blue color (output data file "0.10d" from WAMIT®).

For the computations considering Newman's approximation, the QTF values used were the mean drift pitch moments calculated from the 1st order solution.

Also with respect to the different approximations, the following considerations shall be done for the graphics of Fig. 21:

- Complete QTF matrix—QTF values computed for all pairs of frequencies defined in Section 3.2.1 were employed.
- White-noise approximation—the pitch moment spectral density has constant value for all difference-frequencies and equal to the value for the difference-frequency corresponding to the pitch natural period as showed in Eq. (18).
- Newman's approximation—QTF values for the difference-frequency $\mu = (\omega_i - \omega_j)$ are approximated by the mean drift forces or moments computed for the frequencies $(\omega_i + \mu/2)$, as stated by Eq. (16).

For a better visualization of the influence of the pitch moment QTF on the response spectrum, Fig. 21 also presents a curve representing the square of the unitary moment transfer function normalized in such a way that its peak is always equal to the value of the moment spectrum at the natural frequency.

[3] It is important to emphasize that the wave elevation spectral density also varies with the DOF. Therefore, the significant amplitude pitch numerical results from Table 3 were obtained varying the aliasing of wave spectrum. (DOF = from 4 to 64).

[4] The wave spectrum employed for the results in Fig. 21 was computed with DOF = 22.

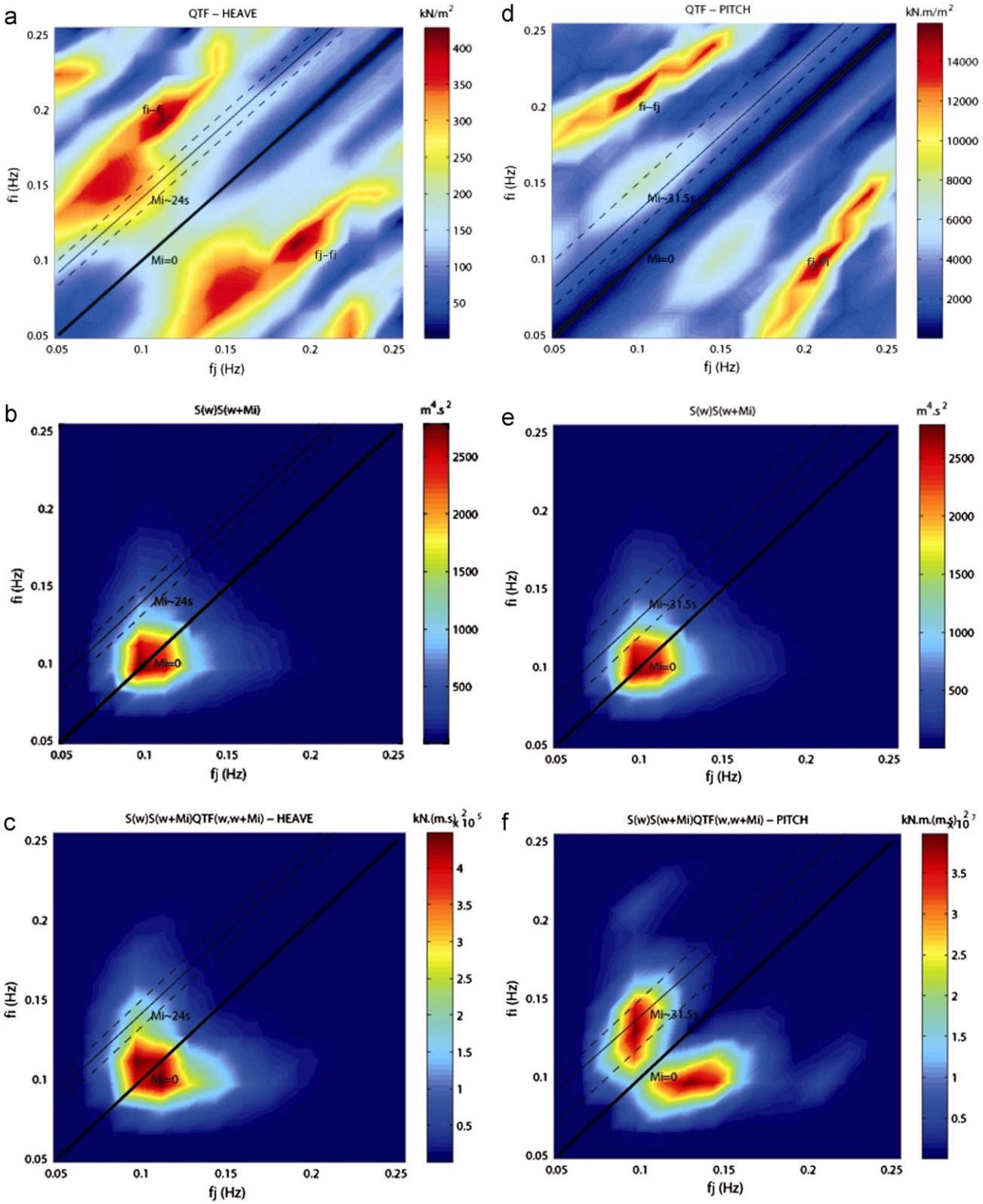

Fig. 17. Values of $|T_{\alpha}^{(-)}(\omega;\omega+\mu)|$, $S(\omega)S(\omega+\mu)$, $S(\omega)S(\omega+\mu)|T_{\alpha}^{(-)}(\omega;\omega+\mu)|^2$ for heave (a, b, c) and pitch (d, e, f), respectively.

Results in Fig. 21 show that the more substantial are the approximations concerning the QTF computations, the lower are the values of the pitch moment spectra. It should be noticed that the approximation that disregards the influence of the 2nd order potential (c) has a much more pronounced effect on the pitch moment spectrum than the one that neglects the free-surface forcing terms in the second-order problem.

Fig. 22 depicts the experimental and numerical computations of the pitch response spectrum. Concerning these results, the following options were tested:

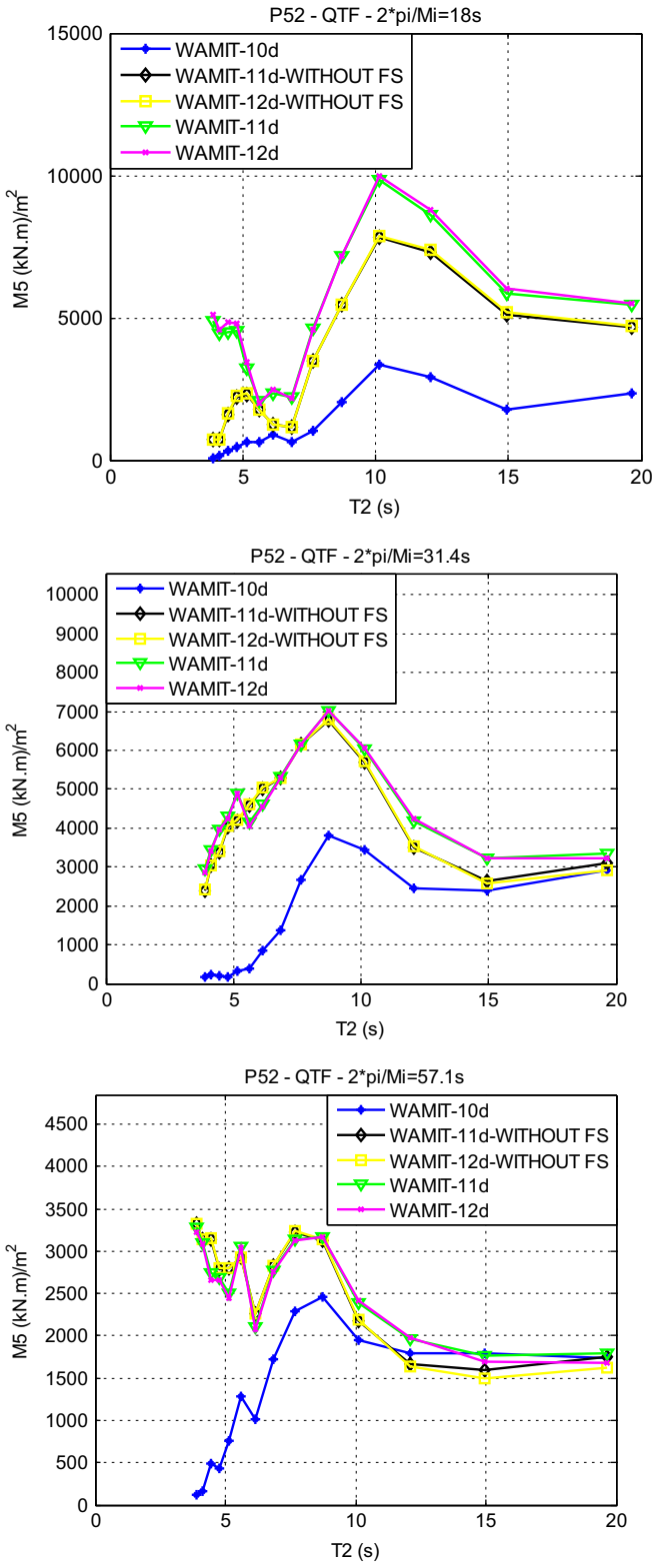

Fig. 18. Pitch moment QTF values computed with different hydrodynamic approximations. (For interpretation of the references to color in this figure legend, the reader is referred to the web version of this article.)

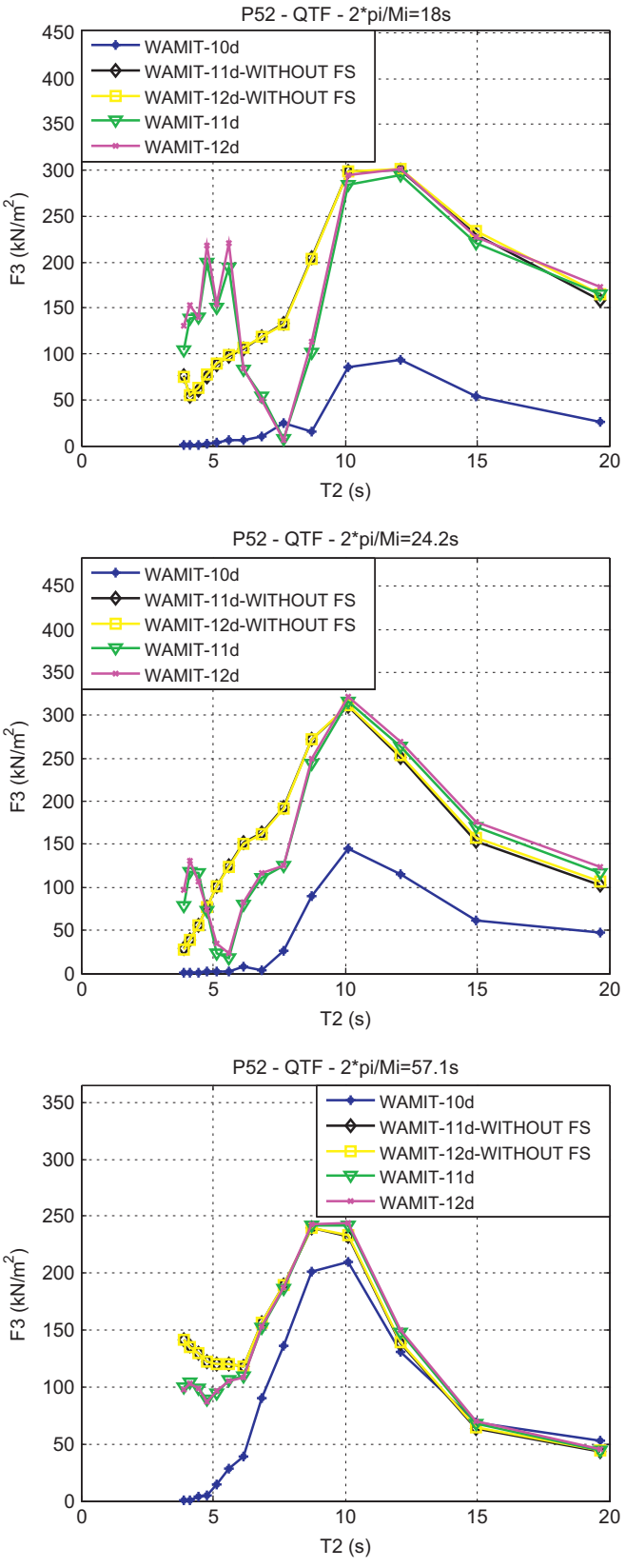

Fig. 19. Heave force QTF values computed with different hydrodynamic approximations.

- NUM. (6dof)—the computation is done as shown in Eq. (22), by employing the second-order RAO ("filename.16d" from WAMIT®). Therefore, in this computations the dynamic couplings between the six degrees of freedom are taken into account.

- NUM. (1dof)—computations are done according Eq. (19), with the QTF matrix ("filename.11d", "filename.12d" or "filename.10d" from WAMIT®) calculated for all difference-frequencies $\mu =$

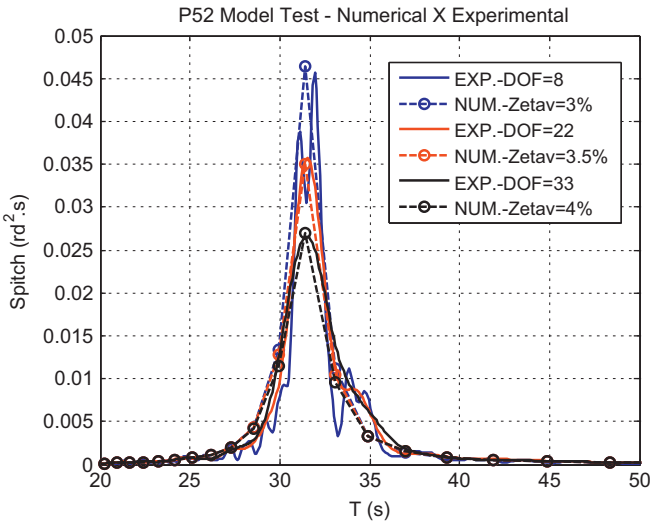

Fig. 20. Comparison of the spectral density function for the pitch response and the numerical computations (using $RAO_5^{(2-)}$ from WAMIT® with the complete second-order potential solution) with varying the viscous damping ratios.

Table 3
Comparison of experimental and numerical results for the significant pitch amplitude with varying ζ_v.

P52 model test—pitch significant amplitude (deg.)							
DOF	**4**	**8**	**16**	**32**	**64**	**Mean (deg.)**	**Dif. (%)**
Experimental	1.242	1.216	1.264	1.236	1.227	1.237	–
NUM.—ζ_v=3%	1.363	1.354	1.387	1.391	1.387	1.376	11.26
NUM.—ζ_v=3.5%	1.240	1.235	1.265	1.269	1.264	1.255	1.42
NUM.—ζ_v=4%	1.147	1.143	1.171	1.175	1.171	1.161	−6.14

$(\omega_i-\omega_j)$ (red curves in Fig. 21). The main difference between this case and the previous one is that the unitary moment transfer function is now approximated by the calculation with 1dof—see Eq. (20). $A_{\alpha\alpha}(\omega)$ and $B_{\alpha\alpha}(\omega)$ are obtained from the output data "filename.1" from WAMIT® and $B'_{\alpha\alpha}$ is the viscous damping value (in this case, ζ_v=3.5%).

- White-noise approximation—the procedure follows Eq. (17) with the QTF values computed only for the difference-frequency corresponding to the pitch natural period $(\omega_i-\omega_j)=\mu_n$ (black curves in Fig. 21). The transfer function $H_\alpha(\omega)$is obtained as explained in NUM. (1dof).
- Newman's approximation—calculation is performed according Eq. (19) with the pitch moment spectrum obtained with Eq. (18) and the QTF values $(T_\alpha^{(-)}(\omega;\omega+\mu))$ approximated by Eq. (16) (using output data "filename.9" from WAMIT®). The transfer function $H_\alpha(\omega)$ is obtained as explained in NUM. (1dof).

One should notice that, as already expected and discussed in Section 2.4.3, the computations based on Newman's approximation present poor agreement with the experimental results. Likewise, the other methods that neglect the second-order potential effects also deviate considerably from the results derived from the experiments. On the other hand, the approximation that includes the second-order potential computed without the quadratic free-surface forcing terms provides quite reasonable results.

When the dynamic model is concerned, the computations that are performed considering only one degree of freedom (1 α and white-noise in Fig. 22) lead to slightly higher significant amplitudes of motion, if compared to those computed by the RAOs including the six degrees of freedom (see Table 4) and considering

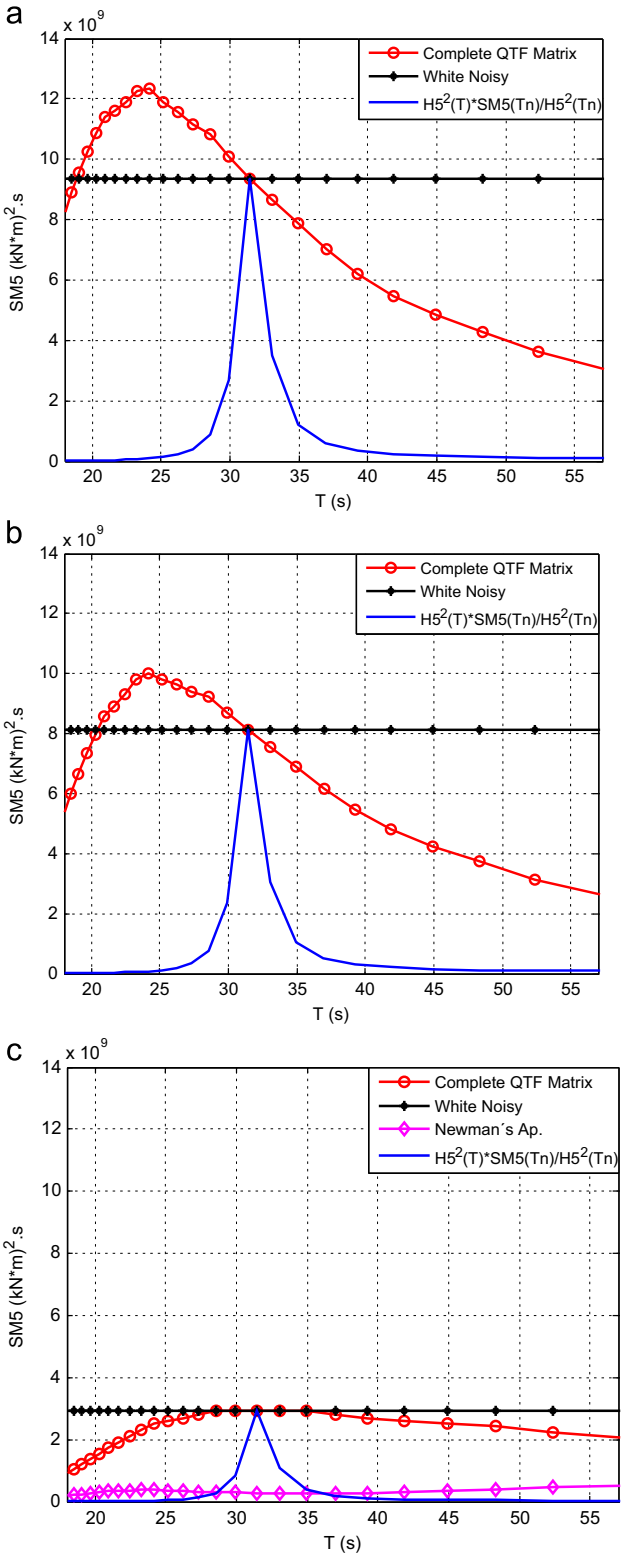

Fig. 21. Comparison of the pitch moment spectral density calculated with different approximations: (a) complete second-order potential; (b) second-order potential without the free-surface forcing term; (c) without second-order potential. (For interpretation of the references to color in this figure legend, the reader is referred to the web version of this article.)

the same viscous damping ratio (ζ_v=3.5% of the critical damping for the corresponding mode). This is a result of the dynamic coupling effects between pitch and other motions. In order to illustrate such effects, Fig. 23 shows the pitch RAO curve computed

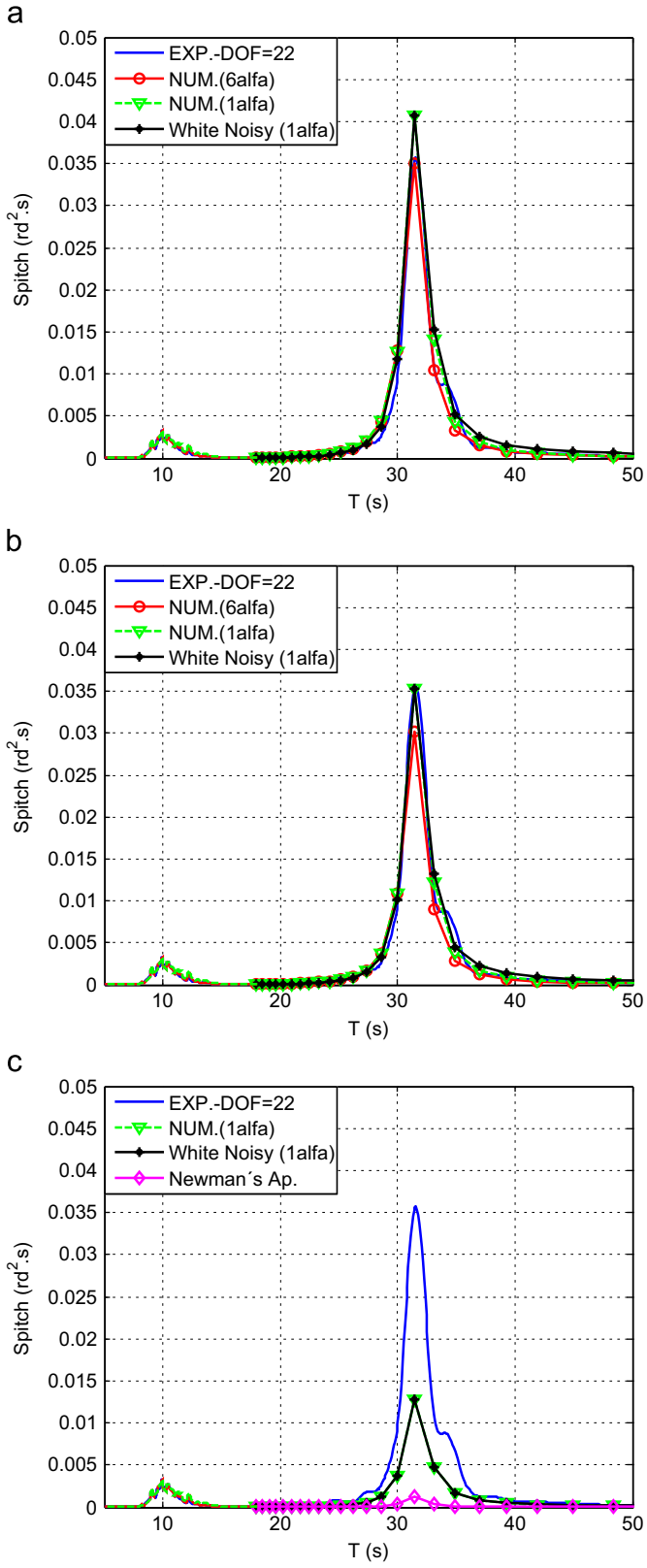

Fig. 22. Comparison of the pitch spectral density experimental result with different numerical approximations (ζ_v=3.5%): (a) complete second-order potential; (b) second-order potential without the free-surface forcing term; (c) without second-order potential.

with the complete mass, damping and stiffness matrixes (6 α—output data "filename.4" from WAMIT®) and the one calculated using only the values in the main diagonal of the same matrixes (1 α—using output data "filename.2" for added mass and potential damping and "filename.1" for wave excitation force from WAMIT®). The disagreement between these two RAO curves makes the coupling effects visible.

Analogous comparisons were performed for the heave motions. In this case, there was a variation of 1.7% in the second-order peak period when comparing the numerical ($T_n \approx 23.7$ s) and experimental ($T_n \approx 24.1$ s) models. The heave response spectrum was also obtained for different levels of viscous damping, as showed in Fig. 24, and the results in Table 5 indicate that the ζ_v=2% provides the best agreement with the experiments (Fig. 25).

Concerning the heave resonant motions, similar conclusions are obtained, although in this case there was a better agreement between the models considering one or six degrees of freedom α in the numerical computations. One may realize by the results in Fig. 26 that the coupling effects are less significant for the heave motions. In fact, this is confirmed by the results in Fig. 27, as the heave RAO curves vary only slightly for both models (Table 6).

4. Conclusions

A theoretical and experimental analysis of the second order resonant heave, roll and pitch motions of a semi-submersible platform was performed using as a case-study the PETROBRAS 52 unit. The hydrodynamic computations were performed in frequency domain using WAMIT®, a commercial seakeeping code based on a boundary-element method. The main focus of the study was on testing different alternatives for performing the required computations and the computational costs associated to these alternatives. All the numerical estimations were confronted with experimental results previously obtained in tests conducted with a small-scale (1:100) model of the P-52 unit in the Marintek ocean basin.

The theoretical background regarding the computation of the second order wave induced loads was briefly reviewed in Section 2. Following Pinkster (1980), the five components of the low-frequency loads are discussed. The formulation for evaluating the low-frequency force spectrum in irregular seas is also presented, emphasizing the large number of frequency combinations that its computation may involve. Aiming at reducing the required computational efforts, the following approximations were considered:

- QTF computed without free-surface forcing terms.
- QTF computed disregarding the contribution of the second-order potential.
- Newman's approximation.
- White-noise approximation.
- Transfer functions computed disregarding dynamic coupling between motions.

Section 3.1 brought some experimental results obtained in the P-52 model tests. Spectral analyses of wave elevation and motion records were performed to demonstrate that, although the spectrum peak and bandwidth in the resonant region may vary with the aliasing of the signals, the zero order moment of the spectrum remains unaffected. This is important since the validations are based on the resonant motions and therefore require the level of viscous damping to be set. This can be done in a proper manner based on the energy of the motion spectrum.

A numerical model of the P-52 unit was created for WAMIT® calculations. Details concerning mesh generation and calibration of the inertial and restoring parameters were given in Section 3.2. By means of this numerical model, the resonant pitch and heave motions could be estimated considering the different

Table 4
Comparison of experimental and numerical results for pitch significant amplitude movement with different calculation approaches and same damping ratio ζ_v=3.5%.

P52 Model test – pitch significant amplitude – ζ_v=3.5%							
	DOF					MEAN (deg.)	DIF. (%)
	4	8	16	32	64		
1st order							
Experimental	0.911	0.908	0.922	0.926	0.923	0.918	–
Numerical-6alfa	0.912	0.907	0.926	0.929	0.926	0.920	0.23
Numerical-1alfa	0.951	0.944	0.965	0.967	0.965	0.958	4.41
2nd order							
Experimental	1.242	1.216	1.264	1.236	1.227	1.237	–
2nd order — full computation							
Numerical-6alfa	1.240	1.235	1.265	1.269	1.264	1.255	1.42
Numerical-1alfa	1.331	1.324	1.356	1.359	1.356	1.345	8.72
Numerical-WN	1.372	1.342	1.374	1.377	1.374	1.368	10.55
2nd order — without free surface							
Numerical-6alfa	1.148	1.145	1.171	1.175	1.170	1.162	−6.10
Numerical-1alfa	1.237	1.232	1.260	1.264	1.260	1.251	1.09
Numerical-WN	1.277	1.251	1.280	1.283	1.279	1.274	2.99
2nd order — without 2nd order potential							
Numerical-1alfa	0.749	0.744	0.762	0.764	0.763	0.756	−38.87
Numerical-WN	0.769	0.751	0.770	0.772	0.771	0.767	−38.03
Numerical-NA	0.235	0.234	0.236	0.237	0.237	0.236	−80.95

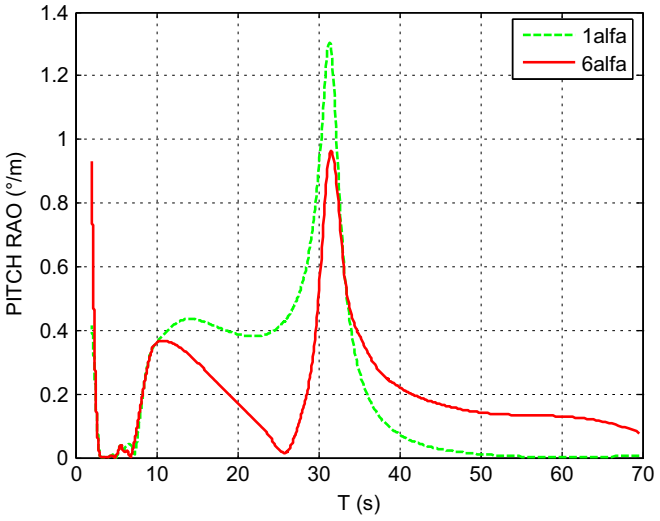

Fig. 23. Pitch RAO calculated with one and six degrees of freedom α (using WAMIT® with ζ_v=3.5%).

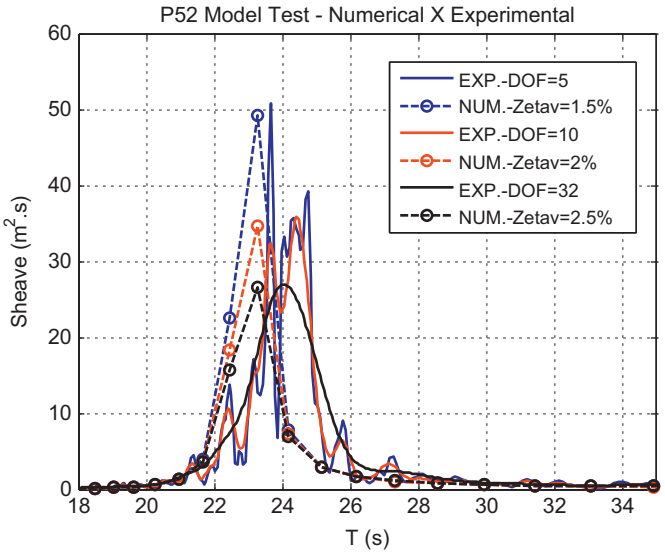

Fig. 24. Comparison of the spectral density function for the heave response and the numerical computation (using $RAO_3^{(2-)}$ from WAMIT® with the complete second-order potential solution) with varying the viscous damping ratios.

approximations mentioned above and, by confronting such estimates to the experimental measurements, the following conclusions were derived:

- Newman's approximation and the one that neglects the second-order potential effects on the second-order loads do not provide accurate estimates for the vertical resonant motions. Indeed, this could be anticipated, given the deep draft of the hull and the relatively low resonant periods of these motions. As a consequence, these approximations are not recommended for the evaluation of slow heave, roll or pitch motions of semi-submersible units.
- For similar hulls, computing the QTFs disregarding the quadratic free-surface forcing terms in the second-order problem seems to be a suitable option for reducing the computational effort. As shown in Figs. 18 and 19, the QTFs for both heave and pitch for low-frequency ranges around the natural frequencies of motions were well reproduced for both, the pitch and heave motions. Consequently, the effects of these terms on the second-order motions resulted quite small.
- The white-noise approximation provided excellent results both for heave and pitch motions. The small discrepancies

Table 5
Comparison of experimental and numerical results for the significant heave amplitude with varying ζ_v.

P52 model test—heave significant amplitude (m)							
DOF	**4**	**8**	**16**	**32**	**64**	**Mean (m)**	**Dif. (%)**
Experimental	0.720	0.709	0.734	0.737	0.744	0.729	–
NUM.—ζ_v=1.5%	0.764	0.766	0.788	0.789	0.787	0.779	6.86
NUM.—ζ_v=2%	0.687	0.689	0.709	0.710	0.708	0.701	−3.85
NUM.—ζ_v=2.5%	0.625	0.626	0.645	0.645	0.644	0.637	−12.60

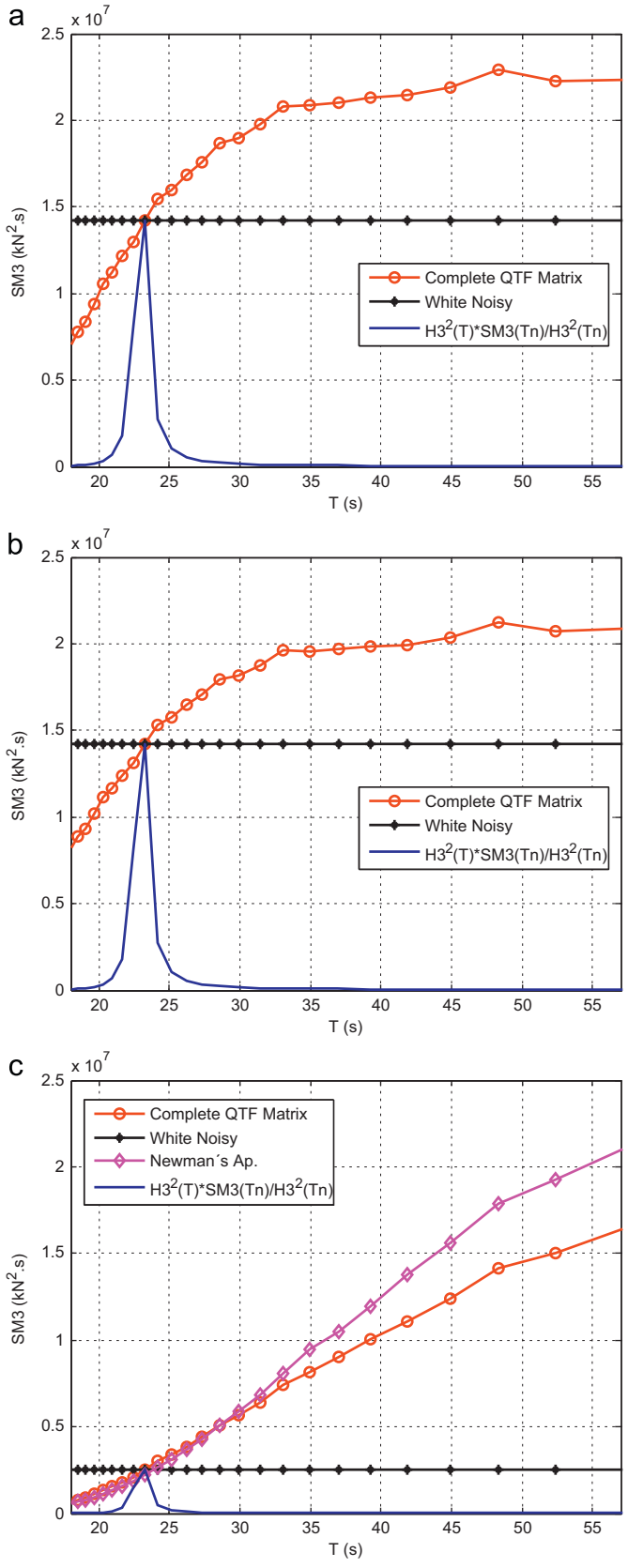

Fig. 25. Comparison of the heave force spectral density calculated with different approximations (ζ_v=2.0%): (a) complete second-order potential; (b) second-order potential without the free-surface forcing term; (c) without second-order potential.

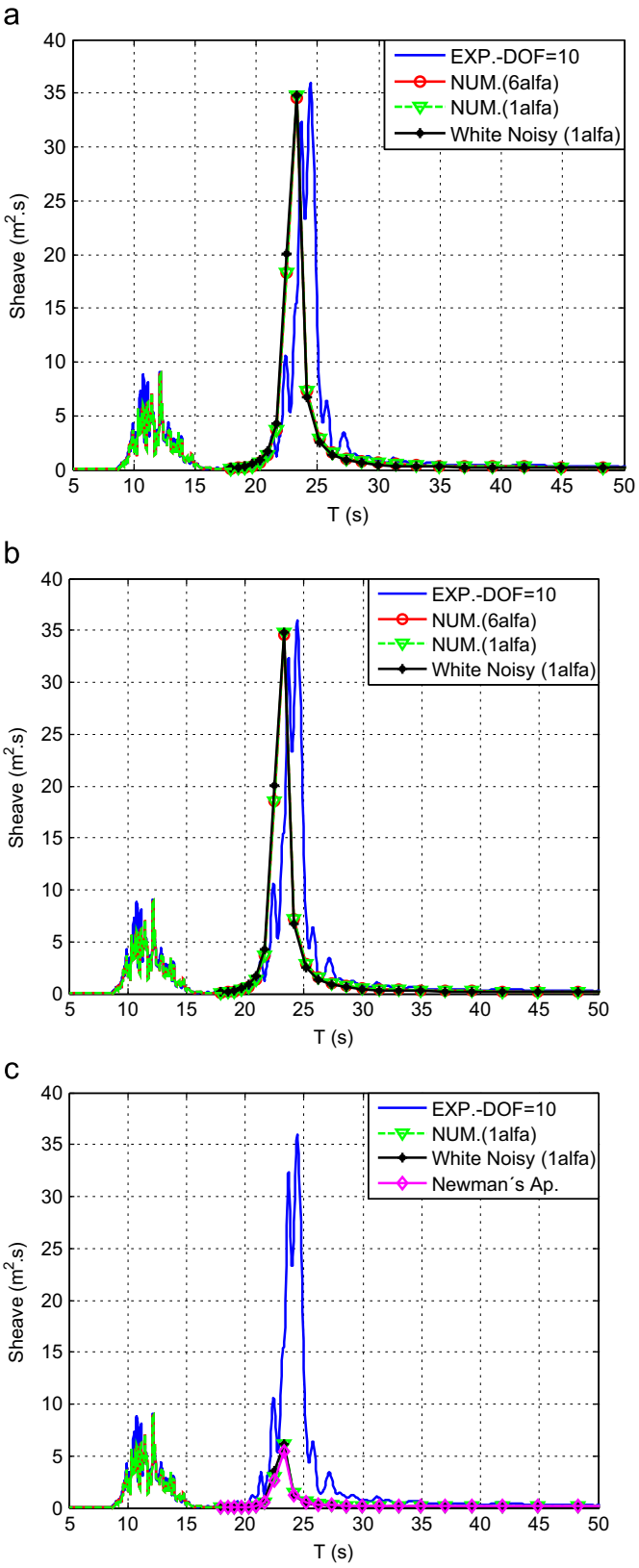

Fig. 26. Comparison of the heave response spectral density experimental result with different numerical approximations (ζ_v=2.0%): (a) complete second-order potential; (b) second-order potential without the free-surface forcing term; (c) without second-order potential.

observed in the results obtained with this approach were found to be associated more to the dynamic model that disregarded the couplings between motions than to the methodology itself. To avoid this, Eq. (17) can be used in the white-noise approach. It is important to emphasize that the computational cost is greatly reduced in this approach,

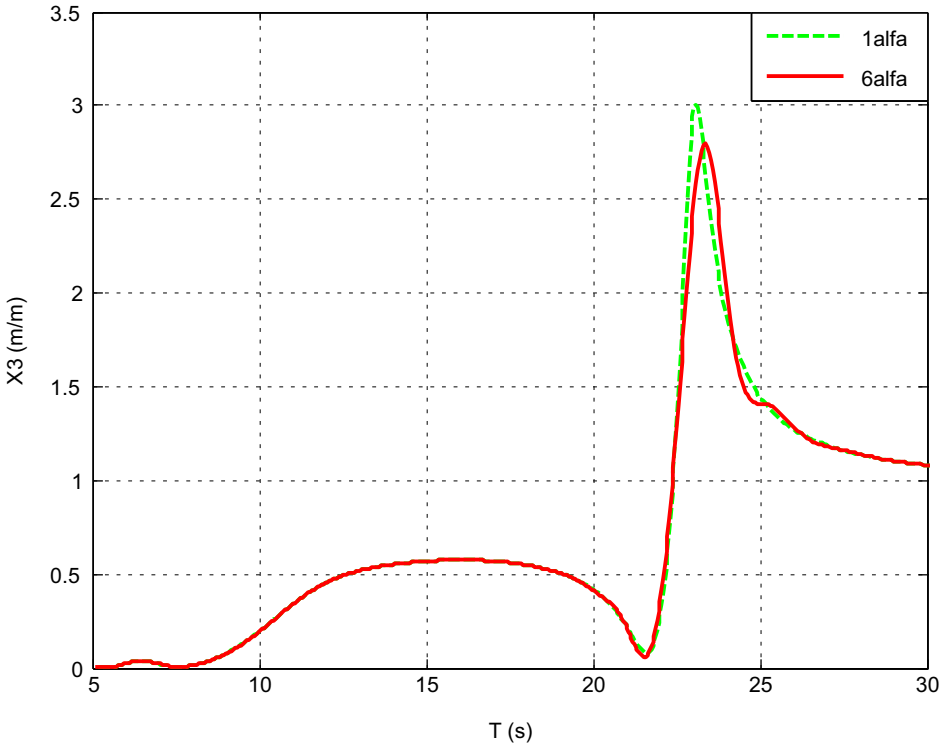

Fig. 27. Heave RAO calculated with one and six degrees of freedom α (using WAMIT® with ζ_v=2.0%).

Table 6
Comparison of experimental and numerical results for heave significant amplitude movement with different calculation approaches and same damping ratio ζ_v=2.0%.

P52 Model test – heave significant amplitude – ζ_v=2%							
	DOF					MEAN (m)	DIF. (%)
	4	8	16	32	64		
1st order							
Experimental	0.739	0.722	0.749	0.741	0.746	0.739	–
Numerical-6alfa	0.786	0.765	0.797	0.787	0.797	0.786	6.33
Numerical-1alfa	0.762	0.741	0.771	0.762	0.772	0.762	2.99
2nd order							
Experimental	0.720	0.709	0.734	0.737	0.744	0.729	–
2nd order — full computation							
Numerical-6alfa	0.687	0.689	0.709	0.710	0.708	0.701	−3.85
Numerical-1alfa	0.688	0.690	0.710	0.711	0.709	0.701	−3.74
Numerical-WN	0.697	0.695	0.713	0.714	0.711	0.706	−3.10
2nd order — without free surface							
Numerical-6alfa	0.687	0.689	0.708	0.709	0.707	0.700	−3.91
Numerical-1alfa	0.688	0.690	0.709	0.710	0.708	0.701	−3.80
Numerical-WN	0.697	0.695	0.712	0.714	0.710	0.706	−3.16
2nd order — without 2nd order potential							
Numerical-1alfa	0.298	0.299	0.308	0.309	0.308	0.304	−58.25
Numerical-WN	0.293	0.292	0.301	0.302	0.300	0.298	−59.15
Numerical-NA	0.290	0.287	0.296	0.294	0.297	0.293	−59.80

since only one frequency difference must be considered. Also, as the damping level of conventional offshore units is generally small, this approach may be envisaged as good alternative for most floating units.

- The decoupled dynamic model provided excellent results concerning the heave motions, but the same accuracy was not observed for the angular motion. In this case-study, the errors involved could be regarded as conservative, since neglecting the coupling effects lead to larger amplitudes of motion, but the same may not be true for different hulls.

All the approximations tested in this case-study contributed to reduce the computational effort involved in the estimation of the second-order resonant motions. This is particularly important in the initial stages of the design, when fast analysis is required. This is also the case when an optimization algorithm is employed to

search for a design with better-quality seakeeping characteristics. Bearing these scenarios in mind, it is important to remind the following:

- When solving the second-order potential problem disregarding the free-surface forcing terms there is no need to discretize the free-surface and this also avoids having to perform somewhat complicated convergence tests.
- The white-noise approach greatly reduces the required number of difference-frequencies, which are limited to the ones corresponding to the natural frequencies of the motions.
- Applying a decoupled dynamic model may further reduce the computational costs, although it should be previously tested for a small number of frequencies in order to evaluate the errors involved.

One should also notice that some of these approximations may be combined. As an example, the resonant heave, roll and pitch motions in the frequency domain may be evaluated with a white-noise approach, employing QTFs computed without the free-surface forcing terms and disregarding the dynamic couplings between the motions. This may be particularly appropriate for accelerating the computations in the initial stages of the design of semi-submersible units.

Finally, it should be reminded that the errors involved in these approximations are dependent on several aspects of the design, such as hull geometry, inertial parameters and viscous damping levels. As a consequence, preliminary tests should be performed for every new design configuration in order to confirm the adequacy of the estimations.

Acknowledgments

The authors would like to thank PETROBRAS for supporting this research, providing all the experimental data and numerical tools employed in this study. Also a special thanks to Prof. Jose Augusto Penteado Aranha and Prof. Johannes Albert Pinkster who gave important suggestions concerning the methodologies appraised in this work.

References

Aranha, J.A.P., Fernandes, A.C., 1994. On the second order low frequency force spectrum. In: Proceedings of Applied Ocean Research. São Paulo, pp. 311–313 (July).

Crandall, H.S., Mark, W.D., 1963. Random Vibration in Mechanical System, Academic Press.

Dallinga, R.P., Huijsmans, R.H.M., Pinkster, J.A., 1988. Combined statistics of first and second order motions of semi-submersibles. In: Proceedings of BOSS Conference. Trondheim, pp. 733–754.

Faltinsen, O.M., Loken, A.E., 1978. Drift forces and slowly varying horizontal forces on a ship in waves. In: Symposium on Applied Mathematics Dedicated to the Late Prof. Dr. R. Timman, Delft, The Netherlands.

Lee, C.H., 1995. WAMIT Theory Manual. Report No. 95-2. Massachusetts Institute of Technology.

Lee, C.H., Newman, J.N., Kim, M.H., Yue, D.K.P., 1991. The computation of second-order wave loads. In: Proceedings of OMAE'91 Conference. v. I-A Offshore Technology. Stavanger, Norway, pp.113–123.

Lee, C.H., Newman, J.N., 2004. Computation of wave effects using the panel method. in: Chakrabarti, S. (Ed.), Numerical Modeling in Fluid-Structure Interaction, WIT Press.

Lighthill,M.J., 1979. Waves and hydrodynamics loading. In: Proceedings of Second International Conference on the Behavior of Offshore Structures (BOSS 79). London.

Marintek Report, 2002. Roncador FPU Model Tests—Main Report. Norwegian Marine Technology Research Institute.

Molin, B., 1979. Second order diffraction loads upon three dimensional bodies. Appl. Ocean Res. 1, 197–202.

MultiSurf®, 2008. User Manual. Version 6.9. AeroHydro, Inc.

Newman, J.N., 1974. Second-order, slowly varying forces on vessels in irregular waves. In: Bishop, R.E.D., Price, W.G. (Eds.), Proceedings of International Symposium on Dynamics of Marine Vehicles and Structures in Waves. Mechanical Engineering Publications, London. pp. 182–186.

Ogilvie, T.F., 1983. Second-order hydrodynamic effects on ocean platforms. In: Proceedings of International Workshop on Ship and Platform Motions. University of California, Berkley.

Pinkster, J.A., 1974. Low frequency phenomena associated with vessels moored at sea. In: European Spring Meeting of SPE-AIME, Paper SPE 4837, Amsterdam, The Netherlands.

Pinkster, J.A., 1980. Low Frequency Second Order Wave Exciting Forces on Floating Structures. Ph.D. Thesis. Technical University of Delft.

WAMIT®, 2006. WAMIT User Manual Versions 6.3, 6.3PC, 6.3S, 6.3S-PC. WAMIT Inc., MA, USA.